

**International Journal of Machining and Machinability of Materials**

ISSN online: 1748-572X - ISSN print: 1748-5711

<https://www.inderscience.com/ijmmm>

---

**Finite element-based study of unidirectional CFRP drilling temperature field**

Hualin Zheng, Zhiwei Hu, Guixin Wang

**DOI:** [10.1504/IJMMM.2024.10061016](https://doi.org/10.1504/IJMMM.2024.10061016)

**Article History:**

Received:	19 October 2022
Last revised:	29 December 2022
Accepted:	01 January 2023
Published online:	18 March 2024

---

## Finite element-based study of unidirectional CFRP drilling temperature field

---

Hualin Zheng\*, Zhiwei Hu and Guixin Wang

School of Mechatronic Engineering,  
Southwest Petroleum University,  
Chengdu, China

Email: zhl@swpu.edu.cn

Email: 1270376369@qq.com

Email: 2282577949@qq.com

\*Corresponding author

**Abstract:** Carbon fibre reinforced resin matrix composite (CFRP) exhibits anisotropy and low thermal conductivity, which facilitates the accumulation of heat produced during drilling. At the hole outlet, the temperature is even higher than the glass transition temperature ( $T_g$ ) of the resin matrix, which is very easy to produce processing damage. In this research, the drilling temperature field model of unidirectional CFRP was established using ABAQUS, and its accuracy was confirmed experimentally. The model is used to examine the temperature fluctuation of the hole wall during drilling. The effect of the high temperature (greater than  $T_g$ ) on the delamination damage, as well as the influence of the processing parameters on the region where the outlet temperature is higher than  $T_g$ . The findings indicate that the temperature of the hole wall is directly linked to the fibre cutting angle. The delamination damage is aggravated in the area where the temperature at the hole outlet is higher than  $T_g$ . The region where the outlet plane temperature is greater than  $T_g$  increases as spindle speed increases, whereas it decreases as feed speed increases.

**Keywords:** CFRP; drilling; temperature field; hole wall temperature; glass transition temperature.

**Reference** to this paper should be made as follows: Zheng, H., Hu, Z. and Wang, G. (2024) 'Finite element-based study of unidirectional CFRP drilling temperature field', *Int. J. Machining and Machinability of Materials*, Vol. 26, No. 1, pp.1–18.

**Biographical notes:** Hualin Zheng is a Professor and Doctoral Supervisor at Southwest Petroleum University. His main research directions are intelligent manufacturing, difficult to machine material cutting theory and processing technology, and composite material processing theory and application. He led or participated in eight national level projects, including National Science and Technology Major Projects, National 863 Plan, National Science and Technology Support Plan, and National Natural Science Foundation of China. He published over 80 academic papers, including nearly 20 indexed by SCI and EI, and authorised nearly ten national invention patents. He has guided more than 50 doctoral and master's students.

Zhiwei Hu is a Master's student at Southwest Petroleum University, majoring in Mechanical Engineering. His main research direction is the drilling technology of composite materials and the finite element simulation of composite materials. He participated in the 'Research on processing damage and process optimisation of Chengfei carbon fiber composite materials' project,

where he was responsible for finite element analysis. He is skilled in modelling software such as CAD, UG, CAE, etc. During his school years, he published a CSCD paper and served as a teaching assistant for undergraduate students.

Guixin Wang is a Master's student at Southwest Petroleum University, majoring in Mechanical Engineering. Her main research direction is milling technology for composite materials and micro finite element simulation of composite materials. The 'Precision machining of gas turbine box parts', she participated in belongs to a major provincial science and technology special project, in which she is responsible for providing finite element technical guidance. During her school years, she published a CSCD paper and was awarded an academic scholarship, serving as a teaching assistant for undergraduate students.

---

## **1 Introduction**

Carbon fibre reinforced resin matrix composites (CFRP) have the performance advantages of high strength, high modulus and light weight, and are widely used in automotive, aerospace and other fields (Geier et al., 2019; Ning et al., 2021). Drilling is often required to meet the requirements of CFRP member connection and assembly. CFRP has the characteristics of low thermal conductivity and temperature sensitivity of resin matrix, which leads to the formation of heat accumulation and high temperature gradient during the drilling process, resulting in processing defects such as thermal damage and tearing of the workpiece material (Davis et al., 2011; Xu et al., 2022).

Researchers have conducted studies on the effect of temperature on the quality of CFRP boreholes. Merino-Perez et al. (2015) investigated the effect of material properties and cutting speed on heat dissipation when drilling carbon fibre reinforced plastic composites using uncoated WC-Co tools. Weinert and Kempmann (2004) and Sorrentino et al. (2017) studied the effect of different cutting parameters on tool temperature and workpiece temperature during drilling of CFRP. Fu et al. (2018) studied the temperature characteristics at the exit of a unidirectional CFRP borehole using an infrared imaging system. Thermomechanical damage such as fibre pullout, burr and peeling was detected at the exit hole wall. Hou et al. (2021b) studied the effect of heat accumulation on cutting temperature and damage by measuring experimental data of hole wall temperature at different fibre cutting angles. Helical milling, ultrasonic assisted machining and other methods proposed by Ning et al. (2021) and Helmy et al. (2020) can reduce the heat accumulation during hole making. Li et al. (2022) explored the influence of thermal damage caused by laser processing on the physical properties of CFRP. The results show that the heat affected zone will weaken the mechanical strength of CFRP, and the influence on tensile strength is relatively small. The main reason for weakening the mechanical properties is that the carbon fibres in the heat affected zone cannot bear the load. Wang et al. (2022) studied the effect of cutting temperature on the quality of CFRP/titanium laminated holes. The results show that a large amount of cutting heat is generated during the cutting process of CFRP and titanium alloy, which leads to a significant increase in the temperature at the CFRP hole outlet. The high temperature reduces the rigidity and bonding properties of CFRP resin matrix, resulting in serious subsurface damage of the fibre layer around the CFRP hole outlet. According to Hancox

(1998) and Fiedler et al. (2013), the mechanical properties of the resin vary greatly when the temperature is below or above the glass transition temperature ( $T_g$ ) of the resin matrix. When the temperature is above  $T_g$ , the modulus and strength will decrease significantly. Therefore, the temperature has an important influence on the machining quality during the drilling of CFRP (Foreman et al., 2010). Meanwhile, researchers have established a temperature field model for drilling CFRP. Chen et al. (2021) used COMSOL to establish a numerical model of the temperature field of drilling unidirectional CFRP to investigate the heat transfer rule during the drilling process. The temperature field model developed by Yang et al. (2019) and Li et al. (2020) equates the heat source of drilling CFRP as a circular planar heat source. Bao et al. (2018) proposed a tapered heat source to simulate the shaped heat source of the drill tip to establish the temperature field model, and the validity of the model was verified by experiments. The study described above enhances the development of the study on CFRP drilling heat. CFRP drilling, on the other hand, results in a complicated temperature field and heat dispersion since the cutting edge is in a semi-closed region and the thermophysical properties of CFRP are anisotropic. In the available literature, there is a minimal investigation of the internal heat transfer process and the formation of a temperature field while drilling unidirectional CFRP. At the same time, we must thoroughly investigate the heat transfer mechanism of anisotropic materials.

This research proposes a uniform heat source model with the same diameter and a specified thickness as the drill bit to replicate the drilling heat source, taking into account heat transfer from the drilling heat source to the hole wall and from the high-temperature drill bit to the workpiece. At the same time, a unidirectional CFRP finite element temperature field model is built, and the moving heat source that is employed to replace the heat produced in the drilling operation is simulated using the DFLUX user subroutine. Experimental results confirm the accuracy of the simulation model. This model is used to analyse the temperature changes at different locations of the hole wall during drilling. The goal of this study is to investigate the impact of processing parameters on the region where the hole outlet surface temperature is greater than  $T_g$ , as well as the connection between this region and outlet delamination damage.

## **2 Drilling temperature field model**

### *2.1 Determination of thermodynamic parameters*

CFRP is made of carbon fibre and resin curing. Fibre direction is lined up in the same direction called unidirectional fibre composite. Due to CFRP anisotropy, the equivalent homogeneous orthogonal anisotropic material assumption is used to simulate unidirectional CFRP. And the following hypothesis is proposed (Chen et al., 2021):

- 1 Close contact between the carbon fibre and the resin matrix, with negligible contact impedance.
- 2 Uniform distribution of carbon fibres in the resin matrix, with no manufacturing defects inside the material.
- 3 The thermal characteristic parameters of CFRP are constant and do not change with temperature.

Equations for calculating the density and specific heat capacity of equivalent homogeneous materials (Liu, 2016) as in equations (1) and (2). The thermal conductivity in parallel and perpendicular to the direction of fibre orientation was estimated using the Wiener model (Mkaddem et al., 2016).

$$\rho = \rho_f \times V_f + \rho_r \times (1 - V_f) \quad (1)$$

$$c = c_f \times V_f + c_r \times (1 - V_f) \quad (2)$$

$$\lambda_{\parallel} = V_f \lambda_f + (1 - V_f) \lambda_m \quad (3)$$

$$\lambda_{\perp} = \frac{\lambda_f \lambda_m}{V_f \lambda_f + (1 - V_f) \lambda_m} \quad (4)$$

$\rho_f$ ,  $c_f$  are the density and specific heat capacity of carbon fibre.  $\rho_r$ ,  $c_r$  are the density and specific heat capacity of epoxy resin.  $\rho$ ,  $c$  are the density and specific heat capacity of unidirectional CFRP composites.  $\lambda_{\parallel}$  and  $\lambda_{\perp}$  are the thermal conductivity of CFRP in parallel fibre direction and vertical fibre direction respectively.  $\lambda_f$  and  $\lambda_m$  are the thermal conductivity of the carbon fibre and the matrix resin, respectively.  $V_f$  is the fibre volume fraction of CFRP. The thermophysical properties of unidirectional CFRP are shown in Table 1.

**Table 1** Thermophysical parameters of unidirectional CFRP

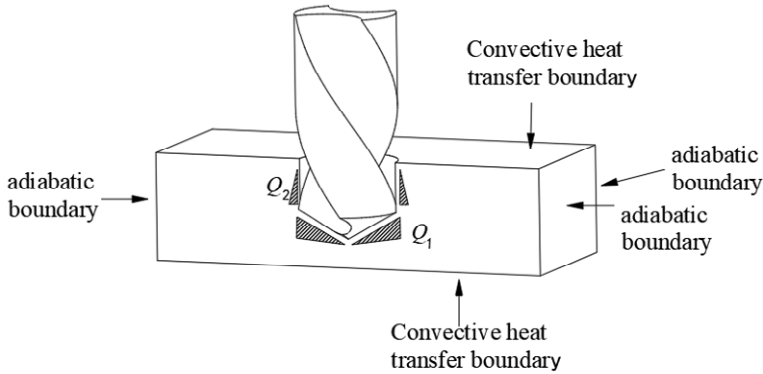
<i>Properties</i>	<i>Value</i>
$\lambda_f$ /(W/(m·K))	10,145
$\lambda_m$ /(W/(m·K))	0.186
$\rho$ /(kg/m <sup>3</sup> )	1,600
$c$ /(J/(kg·K))	465
$V_f$ /%	60
$\lambda_{\parallel}$ /(W/(m·K))	6,161
$\lambda_{\perp}$ /(W/(m·K))	0.282

*Source:* Zhao et al. (2018)

## 2.2 Heat transfer model

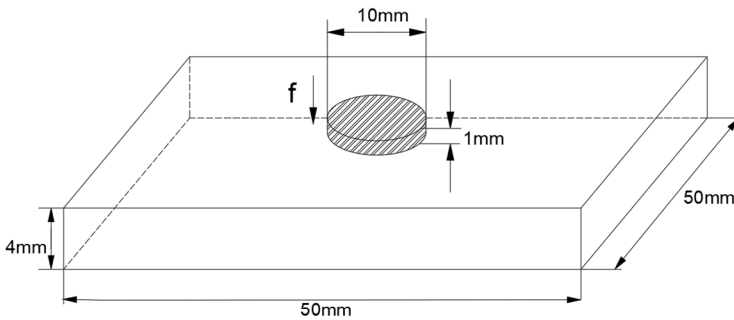
According to the analysis of the characteristics of twist drill machining, the transverse edge and the main cutting edge play a major role in the process of removing materials. The heat source generated by drilling is mainly distributed in the contact area between the main cutting edge of the tool or the cross edge of the tool and the material. The secondary cutting edge is mainly responsible for guiding, so the heat generated by the friction between the secondary cutting edge and the hole wall is small. In Figure 1,  $Q_1$  represents the heat generated by drilling with the main cutting edge and the cross cutting edge, and  $Q_2$  represents the heat generated by drilling with the secondary cutting edge. The heat transferred to the workpiece,  $Q_1 + Q_2$ , comes from the total heat in the drilling process. Since  $Q_2$  is smaller relative to  $Q_1$ , it is neglected here.

**Figure 1** Drilling model boundary conditions



To simplify the model, the heat source generated by drilling is regarded as a uniform cylinder heat source, as shown in Figure 2. The moving speed of the heat source is consistent with the feed speed. The experimental tool used in this paper is as described in Section 2.1: the projection of the main cutting edge on the spindle is 2 mm. The thickness of the heat source should be less than the projection height of the main cutting edge on the main shaft (Chen et al., 2021), so the thickness of the uniform cylinder heat source is one half of the projection height of the main cutting edge. The diameter of the bottom surface of the body heat source is equal to the diameter of the drill bit. The upper and lower surfaces of the model are also considered as thermal convection boundaries. The heat source has very little effect on the front and back left and right four surfaces, so the remaining four surfaces are considered as adiabatic surfaces, as shown in Figure 1.

**Figure 2** Heat source model



Most of the work done by the drill is converted into heat transferred to the chip, tool and workpiece. The total instantaneous heat generated by drilling is the sum of shear heat generation and friction heat generation, expressed by equation (5) (Bono et al., 2002; Denkena et al., 2018). It is assumed that the total heat generated by drilling is  $P$ . The heat transferred to the workpiece is  $Q_0$ . The percentage of heat transferred to the workpiece in relation to the total heat is  $\eta$ . The body heat flow  $q$  (Li et al., 2017) transferred to the workpiece per unit volume, per unit time can be expressed by equation (6).

$$P = Mw + Fv_f \tag{5}$$

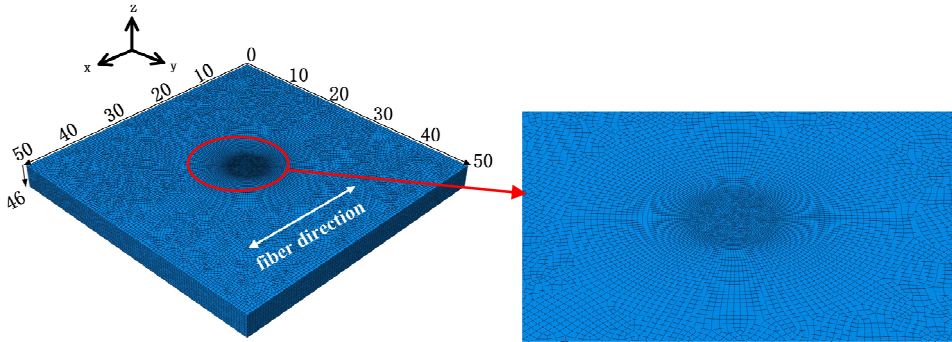
$$q = \frac{Q_0}{V} = \frac{\eta P}{Sh} = \frac{\eta(Mw + Fv_f)}{\pi\left(\frac{d}{2}\right)^2 h} \quad (6)$$

where  $M$  is the torque,  $w$  is the angular velocity,  $F$  is the thrust and is the feed rate.  $V$ ,  $S$ ,  $d$ ,  $h$  are the volume, bottom area, bottom diameter and thickness of the uniform body heat source, respectively.

### 2.3 Temperature field simulation model

The finite element simulation model was built using ABAQUS. The overall model size of the workpiece is a rectangular body of 50 mm × 50 mm × 4 mm. The fibre laying direction of the workpiece is completed by establishing a local coordinate system in the finite element method. The directions  $x$ ,  $y$  and  $z$  represent fibre direction, perpendicular to fibre direction and ply thickness direction respectively. Different fibre direction angles are simulated by changing the direction of direction  $x$ . Figure 3 illustrates the workpiece coordinates with the layout direction of the fibres. The type of cell used for the workpiece is a three-dimensional 8-node linear heat transfer cell (DC3D8). A quadrilateral and sweeping approach is used to divide the grid. The mesh size in the  $x$ - $y$  plane is 0.5 mm. Since the model thickness in the  $z$ -direction is only 4 mm, the mesh size is 0.2 mm. Also, to improve the accuracy of the calculation results, part of the mesh at the heat source loading of the workpiece (central location) was refined. The complete grid cell uses 369,080 cells and 391,776 nodes. The load is applied through a moving heat source defined by the DFLUX user subroutine. The flux size of the heat source is calculated by equation (6). The initial temperature of the workpiece is set to 13.5°C at room temperature. Other boundary conditions are set as shown in Figure 1.

**Figure 3** Simplified model meshing (see online version for colours)



## 3 Drilling experiments and temperature field model validation

### 3.1 Drilling experiment

In order to obtain the heat source loading parameters needed for the simulation model, we completed the drilling CFRP experiment and obtained the axial force and torque for the

drilling process. The experimental procedure is as follows, The drill material used for the experiments was high-speed steel. The diameter of the drill bit is 10 mm and the top angle is 135°. The projection of the main cutting edge on the spindle is 2 mm. The material to be drilled is 4 mm thick T700/epoxy LT03A unidirectional CFRP laminate. The fibre volume fraction and the thermophysical parameters of the workpiece are shown in Table 1.

The drilling is done on a CNC machine. The cutting force is checked by a Kistler 9,272 force measuring instrument. After passing through the Kistler 5080A charge amplifier, the collected data is transferred to the 5697A1 data acquisition card and stored in the computer. The spike wireless cutting force measurement system, model mobile1.2, was used to measure the torque. At the same time, the VarioCAM@hr portable thermal imaging camera from Infotec Germany is placed horizontally to record the temperature values of the drilling process. In order to obtain the drilling temperature values at specific locations in the exit area, this paper adopts a pre-buried K-type thermocouple to record the temperature changes during the drilling process.

**Figure 4** Experimental layout and physical map (a) layout (b) physical map (see online version for colours)

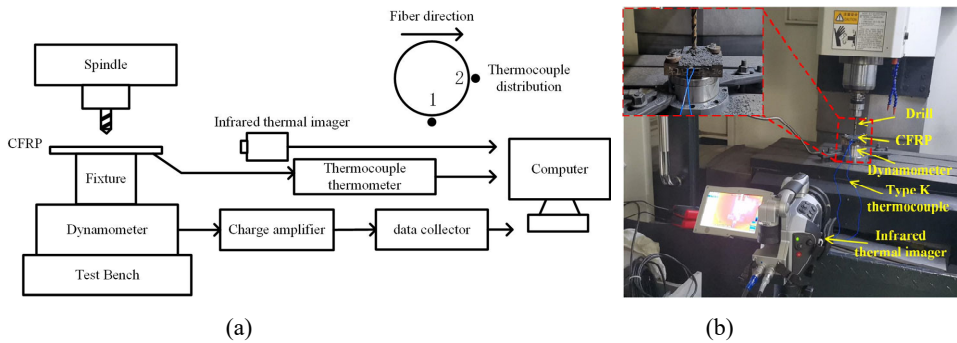
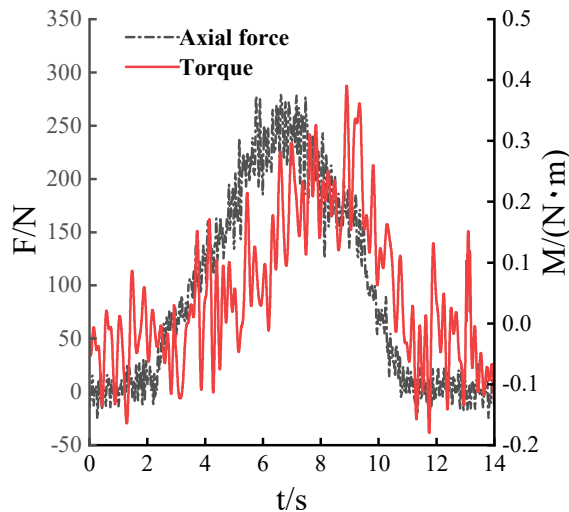


**Figure 5** Experimental thrust and torque of drilling process (see online version for colours)



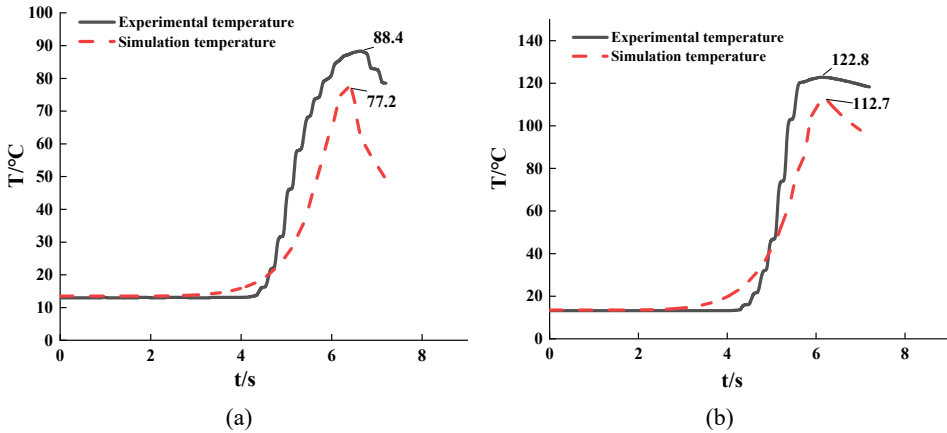
As shown in Figure 4(a) positions 1 and 2 are the thermocouple distribution positions. A blind hole with a diameter of 2 mm is machined in the opposite direction in the area where the thermocouple is distributed on the workpiece. The position of the pre-buried thermocouple is 0.5 mm from the edge of the machined hole. Since defects caused by machining are often found at the exit location of the hole, the thermocouple is buried at a depth of 0.5 mm from the exit surface. The experimental object is shown in Figure 4(b). After the experiment, an industrial microscope was used to observe the exit delamination defects.

### 3.2 Determine heat source loading conditions

The machining parameters are as follows: spindle speed 3,000 r/min, feed rate 50 mm/min. Its drilling axial force and torque variation are shown in Figure 5. From the figure, we can know that the average thrust force of drilling is 225 N and the torque is 0.2 N·m. Bringing the values of thrust force and torque into equation (5) can determine the size of the heat source. Under dry processing, no cooling conditions, the drilling process is considered to take place in a natural convection environment. Convective heat transfer coefficient  $h = 20 \text{ W}/(\text{m}^2 \cdot \text{K})$ .

The temperature value of the workpiece at the drill tip position, measured by the infrared thermography, is brought into the established finite element model when the cross-edge of the drill reaches the exit surface. The heat transferred to the workpiece under this processing condition is derived from equation (6), and the percentage of heat transferred to the workpiece to the total heat,  $\eta$ , is calculated. Calculation results show a percentage of 17%.

**Figure 6** Experimental and simulated temperature rise curves (a) vertical fibre direction (b) parallel fibre direction (see online version for colours)



### 3.3 Model validation

Drilling experiments were conducted using the experimental bench shown in Figure 4(b) and the machining parameters determined in Section 2.2. The temperature data measured by the thermocouple is compared and analysed with the temperature value of the corresponding point in the simulation results. Figure 6 shows the experimental and

simulated temperature trends with time for the two points on the exit side. In the pre-drilling stage, the temperature at the hole exit does not change because less heat is generated. As the drill moves downward, the cutting heat accumulates and the temperature increases until the maximum value, after which the temperature decreases. From the trend of both, it can be seen that the experimental and simulation results change in the same trend. However, there is a slight difference in the trend between the experimental and simulated values at 3 s–6 s. The main reason: the model was built assuming that the CFRP thermophysical parameters are homogeneous, while the experimental material is likely to have defects. There is a slight difference between the actual heat source generated and the heat source that the model reduces to a stable one.

The maximum relative errors between the experimental and simulated temperature profiles at the two measurement points are 12.7 % and 8.2 %, respectively, and the experimental phenomena in the literature '(Bao et al., 2018)' for the above results have a similar pattern of variation. In summary, the simulation results are in high match with the experiments, and the proposed model can be used for the analytical study of unidirectional CFRP drilling temperature field.

## **4 Results and discussion**

### *4.1 Hole wall temperature distribution*

Excessive temperatures generated during the drilling process tend to cause subsurface damage to the hole wall (Hou et al., 2021b). The high temperature causes the resin matrix to melt and bond to the hole walls after cooling, resulting in uneven surfaces and colour changes (Bao et al., 2018). It is necessary to use the simulation model to analyse the hole wall temperature variation pattern. The fibre cutting angle is the angle between the fibre direction and the cutting speed. The fibre cutting angle  $\theta$  at the entrance of the drill hole is shown in Figure 7. In order to study the relationship between hole wall temperature and  $\theta$ , four fibre cutting angles of  $0^\circ$ ,  $45^\circ$ ,  $90^\circ$  and  $135^\circ$  were selected. Then, one measurement point is taken every 0.4 mm along the workpiece thickness direction from the exit plane respectively, and a total of 5 measurement points are taken. The measurement point close to the hole exit is taken because the semi-enclosed environment of drilling makes the heat accumulate, and the closer to the exit position the higher the temperature. The measurement position is shown in Figure 8.

The temperature variation with time at different measurement points is shown in Figure 9. Temperature trend at each point of the hole wall: As the drill moves down, the temperature gradually increases and reaches its maximum value in turn, and finally decreases slightly until the end of drilling. At the same drilling time, compare different  $\theta$  it can be seen that: the measuring point at  $\theta = 0^\circ$  has the lowest temperature value. The temperature value at the  $\theta = 90^\circ$  measuring point is the highest. The reason is the low thermal conductivity in the vertical fibre direction, which makes the heat conduction slow and the temperature rise rate low. While the parallel fibre afferents is directly opposite to the vertical fibre. The change of temperature with time at the measuring point corresponding to the fibre cutting angle of  $45^\circ$  and  $135^\circ$  is similar. This is because the heat transfer is the same for these two fibre cutting angles.

Figure 7 Fibre cutting angle  $\theta$

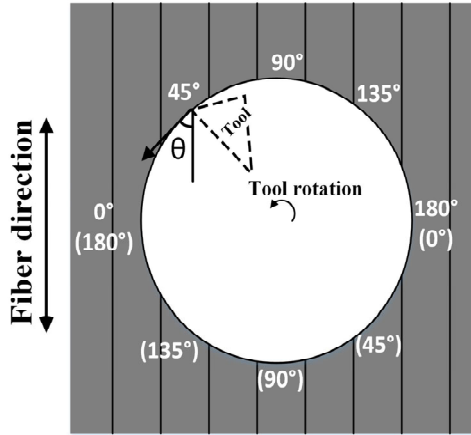
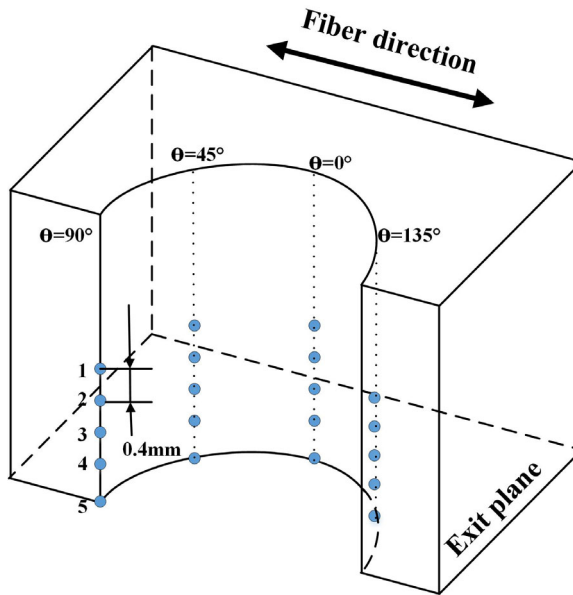


Figure 8 Measurement location (see online version for colours)



The relationship between the maximum temperature of different fibre cutting angles and the measuring position is shown in Figure 10. At the same measuring position of workpiece thickness, different  $\theta$  the highest temperature value of is in the order of  $90^\circ > 45^\circ > 135^\circ > 0^\circ$ . When the  $\theta$  is the same, the closer the position is to the exit surface, the higher the maximum temperature value. This is due to the fact that the heat accumulation is more pronounced the closer you get to the exit surface. At  $\theta = 90^\circ$ , the highest temperature exceeded the  $T_g$  of the resin matrix ( $120^\circ\text{C}$ ) (Hou et al., 2021a) in the area from position 3 to position 5 with a thickness of 0.8 mm during drilling. Excessive temperature will soften the resin matrix in these areas, and the fibre will lose its support,

leading to processing damage such as hole wall sub surface damage, matrix cracking, debonding, etc. (Hou et al., 2021a, 2021b).

**Figure 9** Variation of temperature at different positions on the hole wall with time (see online version for colours)

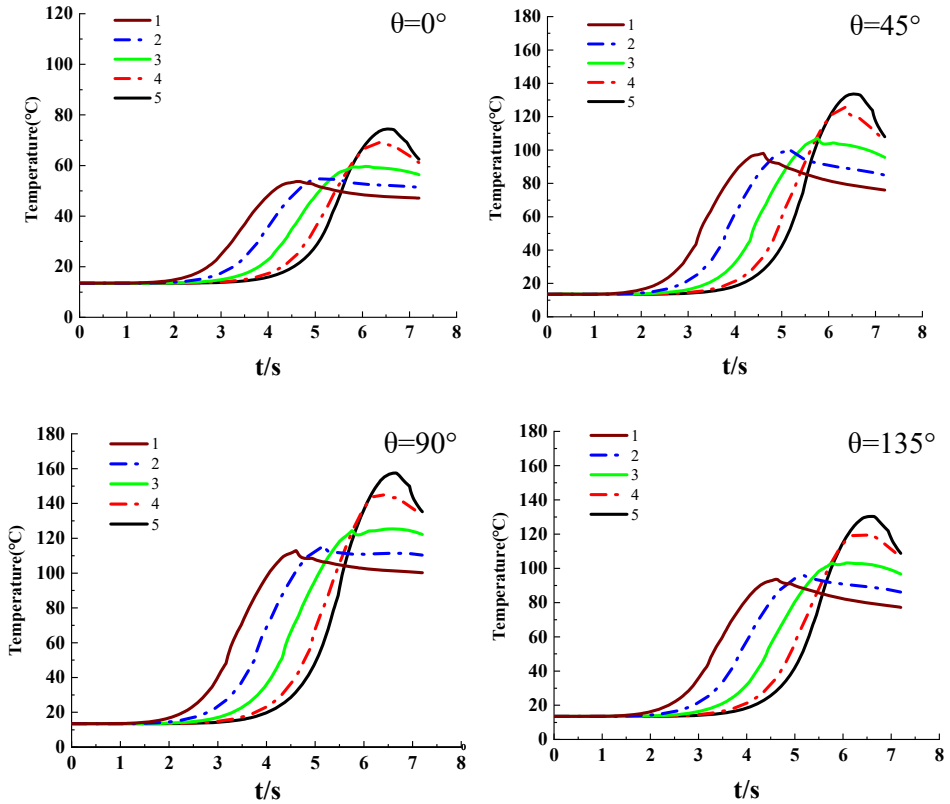
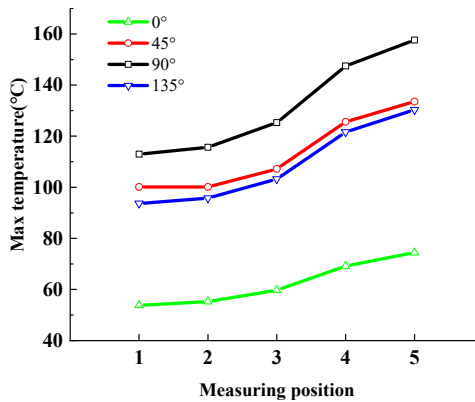


**Figure 10** Maximum temperature at different positions on the hole wall (see online version for colours)

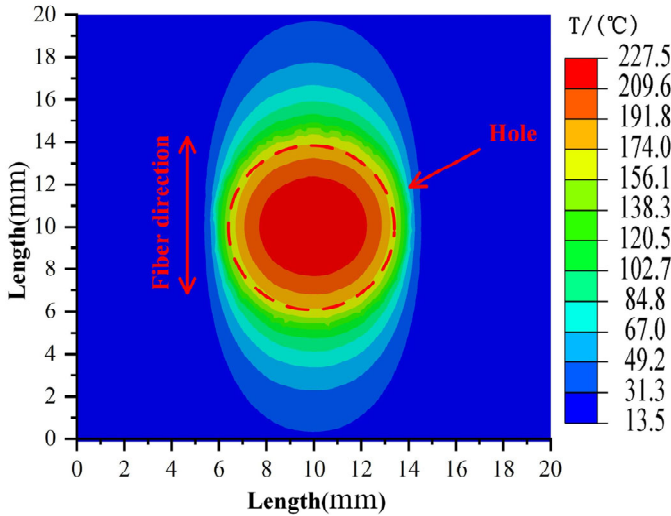


#### 4.2 Effect of hole exit surface temperature above $T_g$ region on delamination damage

When the cross-edge of the drill reaches the exit surface, the local temperature of the exit surface is already higher than the  $T_g$  of the resin matrix due to the accumulation of cutting heat, and the temperature field at the exit is shown in Figure 11. The damage to the exit surface of the experimental workpiece under the same conditions is shown in Figure 12.

In order to compare the region of the hole exit surface temperature above  $T_g$  (high temperature region) with the exit delamination damage. The distance  $L_1$  from the edge of the temperature above the  $T_g$  region to the centre of the hole is obtained every  $10^\circ$  fibre cutting angle along the circumference of the hole in the exit temperature field. The distance  $L_2$  from the maximum delamination edge to the centre of the hole in the interval is obtained at the exit surface of the workpiece along the circumference of the machined hole at  $10^\circ$  fibre cutting angle intervals. The obtained values of  $L_1$  and  $L_2$  are plotted in polar coordinates with the variation of fibre cutting angle as shown in Figure 13.

**Figure 11** Outlet surface temperature field (see online version for colours)



The red shaded part (Hereinafter referred to as high temperature area  $S$ ) consisting of  $L_1$  and  $R$  in Figure 13 indicates the high temperature area other than the hole. At the position of fibre cutting angle of  $90^\circ$ , the high temperature area is widely distributed, and the distribution of adjacent positions gradually decreases. The temperature is lower than  $T_g$  when the fibre cutting angle is near  $0^\circ$  and  $180^\circ$ . The reason for this is that the heat transfer from the unidirectional CFRP workpiece is mainly along the fibre direction, which leads to the difference in temperature at different fibre cutting angles. The yellow shaded portion consisting of  $L_2$  and  $R$  indicates the exit maximum stratification region. As can be seen from the figure, the delamination damage is more serious at the position where the fibre cutting angle is  $90^\circ$ . There is less delamination when the fibre cutting angle is near  $0^\circ$  and  $180^\circ$ .

Figure 12 Surface damage at hole exit (see online version for colours)

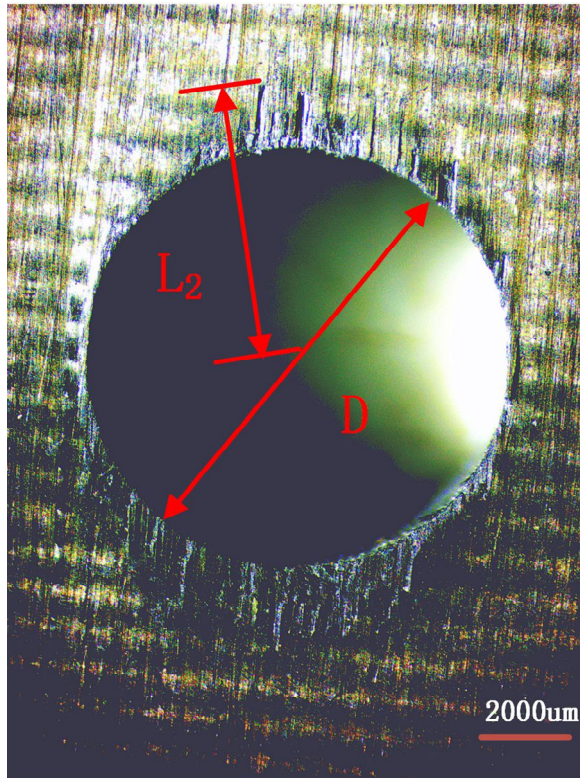
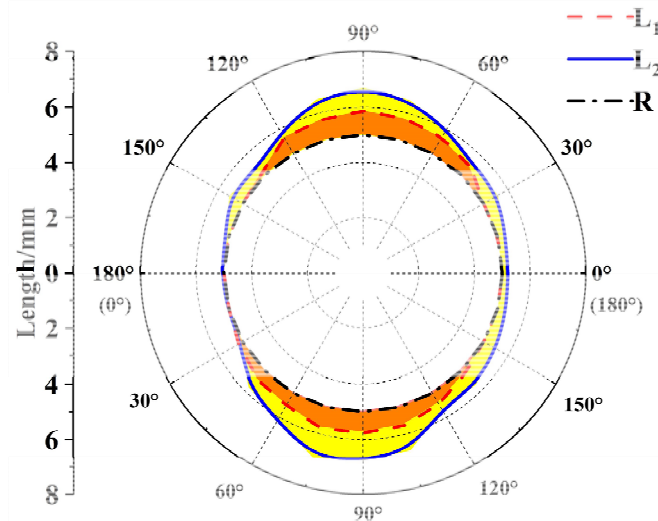
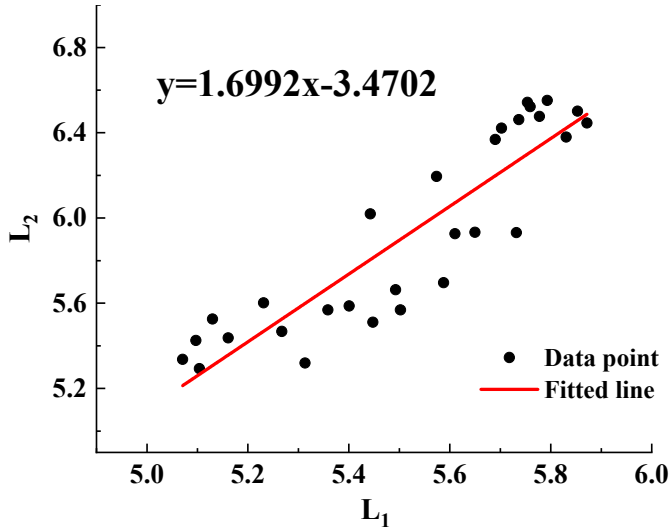


Figure 13  $L_1$ ,  $L_2$  change with  $\theta$  (see online version for colours)



**Figure 14** The variation trend of  $L_2$  with  $L_1$  (see online version for colours)

By comparing  $L_1$  and  $L_2$  in Figure 13, it can be seen that the damage profile of delamination at the hole outlet is highly consistent with the high temperature region profile of the simulated outlet. Delamination damage was most severe near the fibre cutting angle of  $90^\circ$ , while the area of the high-temperature region at this location was the largest. This is because temperatures above  $T_g$  will soften the substrate. When the softened area is cut by the drill, the fibres are more likely to come out and peel off the matrix compared to other areas (Hou et al., 2021a), so delamination damage is more likely to occur.

To investigate the pattern of  $L_2$  variation with  $L_1$ , a regression analysis is established, as shown in Figure 14, where the correlation coefficient is greater than 0.9. It can be seen that the two are linearly correlated and  $L_2$  increases with  $L_1$ . In summary, the delamination damage is exacerbated by the region of higher temperature than  $T_g$  at the hole exit.

#### 4.3 Influence of machining parameters on high temperature region of hole exit surface

It can be seen from Section 3.2 above that the high-temperature area on the hole outlet surface will aggravate the delamination damage. It is necessary to further study the influence of processing parameters on the high-temperature region of the outlet surface. Selection: spindle speed: 3000 r/min, feed speed: 25 mm/min, 50 mm/min, 75 mm/min and feed speed: 50 mm/min, spindle speed: 1,000 r/min, 3,000 r/min, 5,000 r/min, respectively, for drilling unidirectional CFRP. The thrust and torque values obtained from the corresponding drilling experiments are brought into the model to simulate the workpiece temperature field under different processing parameters. The maximum temperature value  $T_{max}$  at the edge of the outlet hole wall and the high temperature area  $S$  at the outlet plane in the temperature field under different processing parameters are

extracted respectively. The variation trend of  $T_{max}$  and  $S$  with spindle speed is plotted in Figure 15. The variation trend of  $T_{max}$  and  $S$  with feed speed is plotted in Figure 16.

Figure 15 shows the influence of spindle speed change on  $T_{max}$  and high-temperature area  $S$ . It can be seen from the figure that  $T_{max}$  and high temperature area  $S$  increase with the increase of spindle speed. The main reason is that with the increase of spindle speed, the number of tool rotations per unit time increases. The number of contact between the tool and the workpiece increases, so the friction between the tool and the hole wall increases, leading to a significant increase in friction heat. With the increase of drilling heat, the workpiece temperature increases, and the high-temperature area  $S$  increases.

Figure 15 Influence of spindle speed on  $T_{max}$  and  $S$  (see online version for colours)

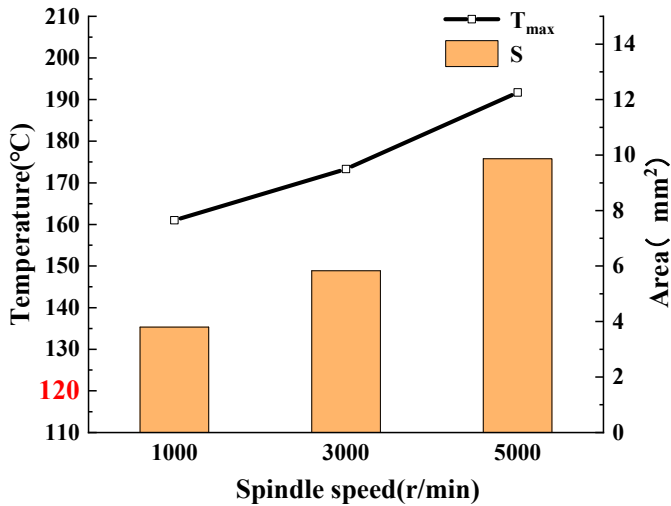


Figure 16 Influence of feed speed on  $T_{max}$  and  $S$  (see online version for colours)

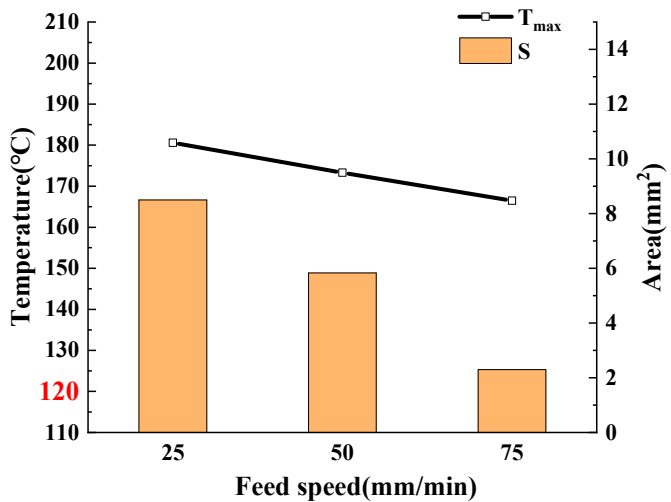


Figure 16 shows the effect of feed speed change on  $T_{max}$  and high-temperature area  $S$ . With the increase of feed speed,  $T_{max}$  and high-temperature area  $S$  decrease. The main reason is that although with the increase of feed speed, the heat generated by the drilling force is increased. But when the material thickness is constant, the feed speed increases and the drilling time decreases, that is, the contact time between the tool and the workpiece decreases. The hole wall generates relatively little heat. The reduction of friction heat generation is greater than the increase of drilling force work heat generation, so the drilling temperature generally shows a downward trend. The drilling temperature decreases, resulting in the reduction of workpiece temperature and the reduction of high temperature area  $S$ .

## 5 Conclusions

In this paper, the CFRP drilling temperature field model is established, and the influence of drilling heat on machining quality is explored by using the model. The following conclusions can be drawn from this study.

- 1 Using ABAQUS, a model of the temperature field during drilling of unidirectional CFRP is established. In this case, the simulation model is quite accurate, with a relative error of 12.7% or less when compared to the experimental data. It can be used to predict and analyse the CFRP drilling temperature field.
- 2 The fibre cutting angle has a significant impact on the rate of hole wall temperature change while drilling carbon fibre-reinforced plastic. Fibre cutting angle  $90^\circ > 45^\circ > 135^\circ > 0^\circ$  is the temperature sequence for the same hole wall thickness.
- 3 On the surface of the borehole outlet, temperatures above  $T_g$  exacerbate delamination damage. The region where the temperature exceeds  $T_g$  is dispersed around the  $90^\circ$  fibre cutting angle, and delamination damage is most severe in this region.
- 4 The region at the CFRP drilling outlet where the temperature is greater than  $T_g$  increases with increasing spindle speeds and decreases with increased feed speeds. Selecting low spindle speed and high feed speed within an acceptable range of processing parameters is beneficial to minimising the region where the temperature is greater than  $T_g$ .

## References

- Bao, Y., Hao, W., Gao, H., Liu, X. and Wang, Y. (2018) 'Numerical and experimental investigations on temperature distribution of plain-woven Aramid fibre-reinforced plastics composites with low-mild spindle velocities', *The International Journal of Advanced Manufacturing Technology*, Vol. 99, Nos. 1–4, pp.613–622.
- Bono, M. and Ni, J. (2002) 'A Model for predicting the heat flow into the workpiece in dry drilling', *Journal of Manufacturing Science and Engineering*, Vol. 124, No. 4, pp.773–777.
- Chen, Y., Li, P., Wang, C., Qiu, X. and Li, S. (2021) 'Numerical simulation and analysis of CFRP drilling temperature field', *Aerospace Materials Technology*, Vol. 51, No. 2, pp.31–37.
- Davis, D.C., Wilkerson, J.W., Zhu, J. and Hadjiev, V.G. (2011) 'A strategy for improving mechanical properties of a fibre reinforced epoxy composite using functionalized carbon nanotubes', *Composites Science and Technology*, Vol. 71, No. 8, pp.1089–1097.

- Denkena, B., MAAß, P., Schmidt, A., Niederwestberg, D. and Gralla, P. (2018) *Thermomechanical Deformation of Complex Workpieces in Milling and Drilling Processes*, Thermal Effects in Complex Machining Processes.
- Fiedler, B., Hobbiebrunken, T., Hojo, M. and Schulte, K. (2013) 'Influence of stress state and temperature on the strength of epoxy resins', *Journal of Applied Physics*, Vol. 95, No. 5, pp.2583–2589.
- Foreman, J.P., Porter, D., Behzadi, S., Curtis, P.T. and Jones, F.R. (2010) 'Predicting the thermomechanical properties of an epoxy resin blend as a function of temperature and strain rate', *Composites Part A: Applied Science and Manufacturing*, Vol. 41, No. 9, pp.1072–1076.
- Fu, R., Jia, Z., Wang, F., Jin, Y., Sun, D., Yang, L. and Cheng, D. (2018) 'Drill-exit temperature characteristics in drilling of UD and MD CFRP composites based on infrared thermography', *International Journal of Machine Tools and Manufacture*, Vol. 135, pp.24–37.
- Geier, N., Davim, J.P. and Szalay, T. (2019) 'Advanced cutting tools and technologies for drilling carbon fibre reinforced polymer (CFRP) composites: a review', *Composites Part A: Applied Science and Manufacturing*, Vol. 125, p.105552.
- Hancox, N.L. (1998) 'Thermal effects on polymer matrix composites: Part 2. Thermal degradation', *Materials and Design*, Vol. 1993-97.
- Helmy, M.O., El-Hofy, M.H. and El-Hofy, H. (2020) 'Influence of process parameters on the ultrasonic assisted edge trimming of aerospace CFRP laminates using MQL', *International Journal of Machining and Machinability of Materials*, Vol. 22, No. 5, pp.349–373.
- Hou, G., Luo, B., Zhang, K., Luo, Y., Cheng, H., Cao, S. and Li, Y. (2021a) 'Investigation of high temperature effect on CFRP cutting mechanism based on a temperature controlled orthogonal cutting experiment', *Composite Structures*, Vol. 268, p.113967.
- Hou, G., Luo, B., Zhang, K., Luo, Y., Liu, P., Cao, S. and Li, Y. (2021b) 'Effects of heat accumulation on the characteristics of hole wall temperature and damages in drilling of UD CFRP', *The International Journal of Advanced Manufacturing Technology*, Vol. 115, Nos. 5–6, pp.1529–1546.
- Li, H. and Song, X. (2017) 'Influence of different heat source models on Q345 medium plate welding temperature field', *Hot Working Process*, Vol. 46 No. 23, pp.205–209.
- Li, H., Ye, Y., Du, T., Zhao, Y., Ren, X. and Hua, Y. (2022) 'The effect of thermal damage on mechanical strengths of CFRP cut with different pulse-width lasers', *Optics and Laser Technology*, Vol. 153, p.108219.
- Li, J., Zou, P., Qiao, C. and Dong, L. (2020) 'Temperature field distribution model in drilling of CFRP/Ti stacks structure', *Journal of physics. Conference Series*, Vol. 1626, No. 1, p.12041.
- Liu, Z. (2016) *Finite Element Analysis of Drilling Process and Research on Drilling Quality of Titanium Alloy/CFRP Laminated Members*, Tianjin University.
- Merino-Pérez, J. L., Royer, R., Ayvar-Soberanis, S., Merson, E. and Hodzic, A. (2015) 'On the temperatures developed in CFRP drilling using uncoated WC-Co tools Part I: workpiece constituents, cutting speed and heat dissipation', *Composite Structures*, Vol. 123, pp.161–168.
- Mkaddem, A., Zain-UI-Abdein, M., Mezlini, S., Bin Mahfouz, A. S. and Jarraya, A. (2016) *Sensitivity of GFRP Composite Integrity to Machining-Induced Heat: A Numerical Approach*, pp.205–214, Springer International Publishing, Cham.
- Ning, H., Zheng, H., Ma, X., Feng, B. and Yuan, X. (2021) 'Prediction of surface roughness and delamination in spiral milling of CFRP laminates by SAPSO-BP neural network', *International Journal of Machining and Machinability of Materials*, Vol. 23, Nos. 5–6, pp.417–433.
- Sorrentino, L., Turchetta, S. and Bellini, C. (2017) 'In process monitoring of cutting temperature during the drilling of FRP laminate', *Composite Structures*, Vol. 168, pp.549–561.
- Wang, B., Wang, Y., Zhao, H. and Wang, M. (2022) 'The effect of cutting temperature on CFRP subsurface during drilling', *Rare Metal Materials and Engineering*, Vol. 51, No. 5, pp.1613–1619.

- Weinert, K. and Kempmann, C. (2004) 'Cutting temperatures and their effects on the machining behaviour in drilling reinforced plastic composites', *Advanced Engineering Materials*, Vol. 6, No. 8, pp.684–689.
- Xu, J., Yin, Y., Paulo Davim, J., Li, L., Ji, M., Geier, N. and Chen, M. (2022) 'A critical review addressing drilling-induced damage of CFRP composites', *Composite Structures*, Vol. 294, p.115594.
- Yang, F., Wang, F. and Jia, Z. (2019) 'Research on calculation of temperature field in CFRP/Titanium Alloy lamination drilling', *Mechanical and Electrical Engineering*, Vol. 36, No. 12, pp.1261–1265.
- Zhao, Y., Song, L., Li, J. and Jiao, Y. (2018) 'Comparison of thermal response mechanisms of 3D woven carbon fibre/epoxy resin composites under two measurement methods', *Journal of Composite Materials*, Vol. 35, No. 1, pp.103–109.